Modeling and Vector Control of Planar Magnetic Levitator

Won-jong Kim, *Member, IEEE*, David L. Trumper, *Member, IEEE*, and Jeffrey H. Lang, *Fellow, IEEE*

***Abstract*— We designed and implemented a magnetically levitated stage with large planar motion capability. This planar magnetic levitator employs four novel permanent-magnet linear motors. Each motor generates vertical force for suspension against gravity, as well as horizontal force for drive. These linear levitation motors can be used as building blocks in the general class of multi-degree-of-freedom motion stages. In this paper, we discuss electromechanical modeling and real-time vector control of such a permanent-magnet levitator. We describe the dynamics in a dq frame introduced to decouple the forces acting on the magnetically levitated moving part, namely, the platen. A transformation similar to the Blondel–Park transformation is derived for commutation of the stator phase currents. We provide test results on step responses of the magnetically levitated stage. It shows 5-nm rms positioning noise in x and y, which demonstrates the applicability of such stages in the next-generation photolithography in semiconductor manufacturing.**

***Index Terms*— dq theory, linear permanent-magnet motor, magnetic levitation, photolithography, precision position control, vector control.**

I. Introduction

MANY traditional mechanical stages for x–y positioning, such as used in wafer steppers in semiconductor manufacturing, have either crossed-axis-type or gantry-type configurations [1]–[3]. The x-axis linear stage is typically driven by another y-axis stage moving orthogonally to the x axis. The mechanical bearing tolerance for these precision position control systems must be very tight, so they are expensive to make. Some precision planar positioners also use a piezoelectric fine-motion stage on top of a coarse x–y mechanical stage. Vertical (z axis) motions for focusing are generated by additional independent mechanical means. Such systems are complicated and expensive and have complex dynamics which limit high-speed operation.

It is a trend that the industry has come to use planar motors for two-dimensional positioning applications more frequently than ever. The Sawyer motor is one of the earliest inventions in this category [4]. Since its motion is tightly constrained to a plane, a Sawyer motor cannot provide focus range or local leveling without using fine-motion actuators. However, the magnetically levitated stage presented herein can generate all six-degrees-of-freedom (6-DOF) motions required for focusing and alignment, and large planar motions for positioning using a single magnetically levitated moving part, namely the platen. This is a significant advance over other existing techniques described previously, thanks to the resulting mechanical simplicity. The platen can be designed to have a high natural frequency and, thus, can be moved more rapidly than multi-element stages which have more complex dynamics. This allows higher speed and, thus, increases machine throughput. Magnetic levitation can also achieve the nanometer-order position resolution required for deep-submicrometer lithography when appropriate position sensors are used.

The actuators for this planar magnetic levitator are three-phase surface-wound surface-permanent-magnet linear motors. Error motions due to cogging and nonlinear effects are expected to be minimal [5]. The linear motor uses a Halbach magnet array for its power efficiency and low field distortion [6], [7]. Induction motors are avoided, since they dissipate heat in the moving part and are generally hard to control. Variable-reluctance motors, such as stepper motors, have inevitable cogging forces. Multiphase permanent-magnet motors are capable of generating suspension force, as well as drive force [8], [9], so that they do not need any other actuators for suspension and fine position adjustments.

We provided a general design and analysis framework for permanent-magnet machines in a previous paper [10]. There, we derived field solutions, force equations, and an electrical terminal relation for a general class of surface-wound linear permanent-magnet motors. Here, we use these results to derive dynamic equations of motion and a commutation law for the planar magnetic levitator.

In this paper, we discuss the modeling and vector control of our planar magnetic levitator. In Section II, we present an overview and the basic working principles of the magnetically levitated stage. A lumped decoupled model using dq decomposition theory is presented in Section III. We derive in Section IV linearized dynamic equations of motion of the magnetically

Paper IPCSD 98–51, presented at the 1997 Industry Applications Society Annual Meeting, New Orleans, LA, October 5–9, and approved for publication in the IEEE TRANSACTIONS ON INDUSTRY APPLICATIONS by the Electric Machines Committee of the IEEE Industry Applications Society. This work was supported in part by Sandia National Laboratories under Subcontract AH-4243. The work of W. Kim was supported by the Korean Ministry of Education. The work of D. L. Trumper was supported by a National Science Foundation Presidential Young Investigator Award. Manuscript released for publication July 9, 1998.

W. Kim is with SatCon Technology Corporation, Cambridge, MA 02142 USA (e-mail: wjkim@alum.mit.edu).

D. L. Trumper is with the Department of Mechanical Engineering, Massachusetts Institute of Technology, Cambridge, MA 02139 USA.

J. H. Lang is with the Department of Electrical Engineering and Computer Science, Massachusetts Institute of Technology, Cambridge, MA 02139 USA.

Publisher Item Identifier S 0093-9994(98)08113-4.

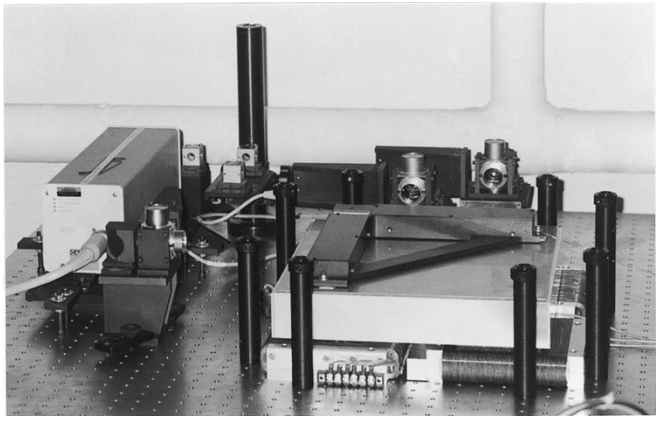

Fig. 1. Planar magnetic levitator.

levitated stage. Finally, the real-time controller design and test results are presented in Section V.

II. Planar Magnetic Levitator

Fig. 1 shows a photograph of the planar magnetic levitator [11]. The planar motion coverage of the stage is 50 mm × 50 mm, which can readily be scaled to accommodate the next generation wafers. For focusing and alignment, the vertical travel range is ±200 μm and the angular ranges of the stage are ±600 μrad. We use three channels of laser interferometers with subnanometer resolution to measure the position in the plane and three channels of capacitance probes for the stage position out of the plane. Thus, all motions required for photolithography can be supplied by this single stage. The design is also applicable to the newer classes of step-and-scan lithography stages.

Fig. 2 is a perspective view of the prototype magnetically levitated stage. The magnetic levitator contains four three-phase linear permanent-magnet motors as its actuators. The linear motor is designed to generate suspension (vertical) force, as well as translational (lateral) force, as indicated in Fig. 2. The unprimed xyz frame (the inertial frame) is fixed to the stators with its origin at the center of the stators on the plane enclosing the three sensing surfaces of the capacitance probes. The primed $x'y'z'$ frame (the body frame) is fixed to the platen with its origin at the platen center of mass.

With an arrangement of the motors as in Fig. 2, the platen generates all 6-DOF motions for focusing and alignment and large two-dimensional step-and-hold and scanning motions for high-precision positioners, as used in wafer stepper stages in semiconductor manufacturing. For example, we actuate positive f_{2y} and f_{4y} in Fig. 3 to get a motion in the positive y direction.[1] To generate a positive rotation around the y axis, we put positive f_{1z} and f_{4z} and negative f_{2z} and f_{3z}. Motions in the four other degrees of freedom are generated in similar ways.

A TMS320C40 digital signal processor is used as a real-time control processor to stabilize and control the planar magnetic levitator. To drive the motors, we constructed linear transconductance power amplifiers. Their maximum current and voltage ratings are ±1.5 A and ±22 V, respectively. The nominal power dissipation per motor is 5.4 W at the 0.5-A nominal peak phase current. The suspension power dissipation coefficient of the magnetically levitated stage is 7.2 mW/N^2. The nominal airgap clearance between the magnet array and the stator is 250 μm. The nominal motor airgap for the capacitance gap sensor is 250 μm larger than that of the motor airgap, so that the capacitance probes are not touched by the platen in any condition. The detailed electrical and mechanical design of the platen and stators and the instrumentation structure of the system are described in [11].

[1]The capital XYZ frame is fixed to the platen and used as a reference frame for the equilibrium conditions in the Appendix. The X and Y axes are on the same plane that contains the x' and y' axes and are rotated by 45° around the z' axis.

III. Decoupled Force Equations

For modeling purposes, we measured the mechanical and electrical parameters of the stage. The platen mass M is measured as 5.58 kg. The inertia tensor of the platen about the platen center of mass is calculated as

$$\boldsymbol{I}_{CM} = \begin{bmatrix} 0.0541 & 0.00276 & -0.00253 \\ 0.00276 & 0.0541 & -0.00261 \\ -0.00253 & -0.00261 & 0.0981 \end{bmatrix} \text{kg-m}^2. \quad (1)$$

The resistance and the self-inductance of one phase of the winding are 14.4 Ω and 3.44 mH, respectively; the mutual inductance is negligible because the stator is ironless. In the rest of this section, we derive decoupled force equations with a dq theory.

A. dq Decomposition

The dq decomposition in conventional rotary machines is introduced to isolate the stator current component that generates torque [12], [13]. The principal goal of the dq decomposition is to express the electrical dynamics of the stator and the rotor in a common reference frame. The direct axis (d axis) and the quadrature axis (q axis) are fixed to the rotor frame and rotate with the rotor. Then, force equations and commutation described in the dq frame do not contain the position dependence with respect to the stator.

Each linear motor in our levitator is designed to generate suspension force, as well as translational force, as indicated in Fig. 2. Decoupling the two orthogonal force components should be performed to control the two degrees of freedom independently. As in Fig. 4, we define the d axis as the z' axis in the platen frame. The q axis leads the d axis by a quarter of the motor pitch, which is 90° in electrical angle, in the $+y$ direction.

In previous work [10], we defined J_a and J_b as the real and imaginary parts of the fundamental current density components in the stator windings. Let J_q and J_d be the quadrature and direct components of this current density, respectively. Then, the following transformation from $[J_a \quad J_b]^T$ to $[J_q \quad J_d]^T$ holds with the definitions in Fig. 4:

$$\begin{bmatrix} J_q \\ J_d \end{bmatrix} = e^{\gamma_1 y_0 J} \begin{bmatrix} J_a \\ J_b \end{bmatrix} \quad (2)$$

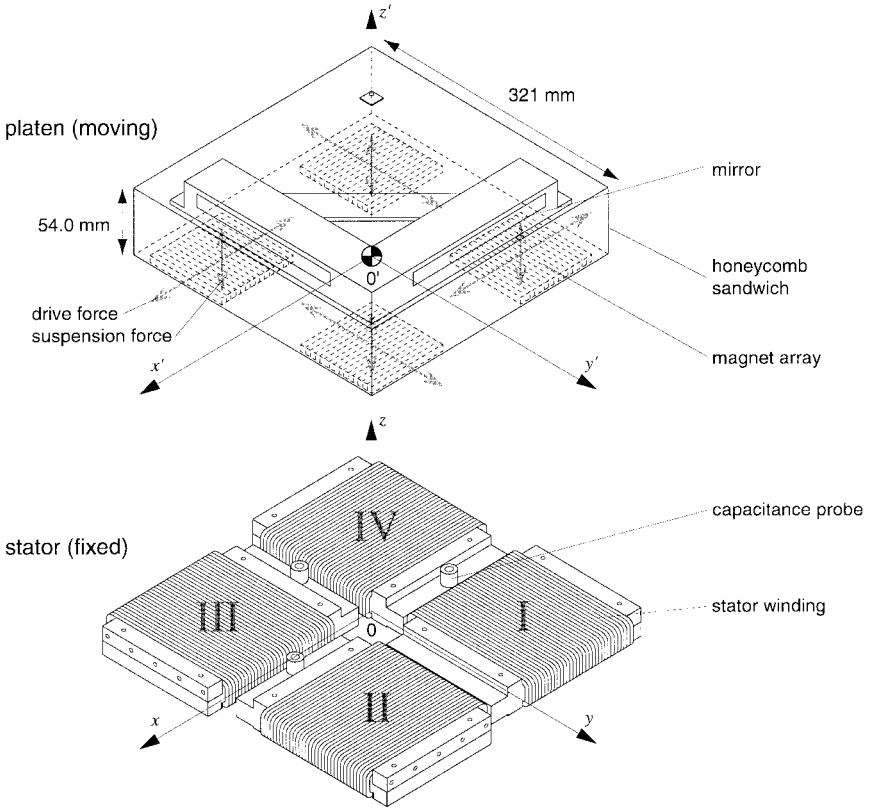

Fig. 2. Perspective view.

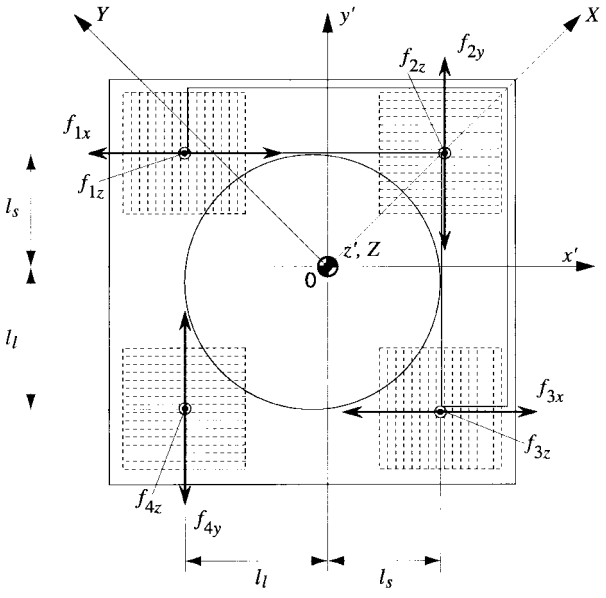

Fig. 3. Free body diagram for force allocation.

where $\gamma_1 = 2\pi/l$, and $e^{\gamma_1 y_0 J}$ is a transformation matrix given by

$$e^{\gamma_1 y_0 J} = \begin{bmatrix} \cos \gamma_1 y_0 & \sin \gamma_1 y_0 \\ -\sin \gamma_1 y_0 & \cos \gamma_1 y_0 \end{bmatrix} \tag{3}$$

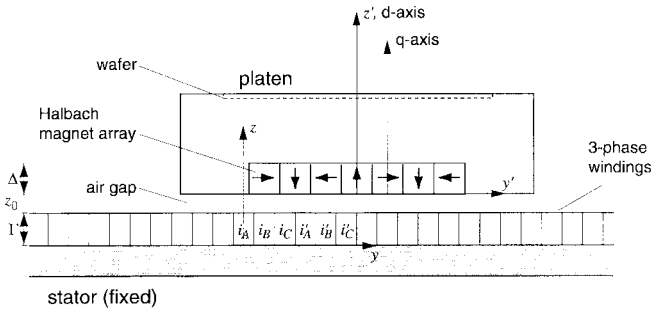

Fig. 4. dq frame fixed to the platen.

and

$$J = \begin{bmatrix} 0 & 1 \\ -1 & 0 \end{bmatrix}. \tag{4}$$

In the above equations, y_0 is the horizontal displacement of the $x'y'z'$ frame with respect to the xyz frame in Fig. 4.

B. Force Equations

We derive decoupled force equations in steady-state suspension in a dynamic equilibrium. Using the relationships $f_{y,z} = N_m f_{(y,z)\lambda}$ and $i_{a,b} = 2\eta_0 J_{a,b}$, we rewrite the relationship [10, eq. (20)] between the total lateral and vertical forces f_y and f_z and the peak current components i_a and i_b. For motors II and IV, this results in

$$\begin{bmatrix} f_y \\ f_z \end{bmatrix} = \tfrac{1}{2}\mu_0 M_0 \eta_0 N_m G e^{-\gamma_1 z_0} \begin{bmatrix} \cos \gamma_1 y_0 & \sin \gamma_1 y_0 \\ -\sin \gamma_1 y_0 & \cos \gamma_1 y_0 \end{bmatrix} \begin{bmatrix} i_a \\ i_b \end{bmatrix}. \tag{5}$$

For our design, the parameters have the following values: the magnet remanence is $\mu_0 M_0 = 1.29$ T; the winding turn density is $\eta_0 = 2.491 \times 10^6$ turns/m^2; the number of active magnet pitches is $N_m = 15/4$; the pitch is $l = 25.6$ mm; the absolute value of fundamental wave number is $\gamma_1 = 2\pi/l = 245$ m^{-1}; the magnet array width is $w = 92.0$ mm; and the nominal motor airgap is $z_0 = 250$ μm. The magnet array thickness is $\Delta = l/4$ and the winding thickness is $\Gamma = l/5$, determined via the power optimal design presented in [7]. The constant G contains the effects of the motor geometry and is equal to 4.89×10^{-6} m^3 [10]. The same force equation is valid for motors I and III by changing the variable y_0 to x_0.

From (2) to (5), we can decouple the lateral and vertical force components in the quadrature and direct current components i_{kq} and i_{kd}:

$$f_{k(x,\,y)} = \tfrac{1}{2}\mu_0 M_0 \eta_0 N_m G e^{-\gamma_1 z_0} i_{kq} \tag{6}$$

$$f_{kz} = \tfrac{1}{2}\mu_0 M_0 \eta_0 N_m G e^{-\gamma_1 z_0} i_{kd} \tag{7}$$

where k represents motors I–IV. With the motor airgap z_0 fixed, the lateral and vertical forces are determined by multiplication of the constant magnet residual flux density $\mu_0 M_0$ and the stator currents i_{kq} or i_{kd}.[2] Thus, we produce f_{kz} with i_{kd} and $f_{k(x,\,y)}$ with i_{kq}. The quadrature current i_{kq} does not influence the vertical force f_{kz}, and the same holds for i_{kd} and $f_{k(x,\,y)}$. Substituting the above parameter values specific to our motors,

$$\begin{bmatrix} f_{k(x,\,y)} \\ f_{kz} \end{bmatrix} = 27.7 \text{ N/A} \begin{bmatrix} i_{kq} \\ i_{kd} \end{bmatrix} \tag{8}$$

yield the motor horizontal and vertical forces.

C. Commutation

We derive the commutation for the three-phase current densities J_A, J_B, and J_C in the context of the dq theory (Fig. 4). The stator current density is a function of the lateral position y on the stator frame. We can show that

$$J_x(y) = 2J_a \cos \gamma_1 y + 2J_b \sin \gamma_1 y. \tag{9}$$

The three-phase current densities J_A, J_B, J_C, J'_A, J'_B, and J'_C are located on the stator, the boundaries of which are at $z = 0$, $l/6$, $l/3$, $l/2$, $2l/3$, $5l/6$, and so forth, and $J_A = -J'_A$, $J_B = -J'_B$, and $J_C = -J'_C$. Then, the inverse Blondel–Park transformation holds between $[J_a \quad J_b]^T$ and $[J_A \quad J_B \quad J_C]^T$ in the balanced three-phase operation [14]. From this, it follows that

$$\begin{bmatrix} J_A \\ J_B \\ J_C \end{bmatrix} = \begin{bmatrix} 2 & 0 \\ 2\cos\dfrac{\pi}{3} & 2\sin\dfrac{\pi}{3} \\ 2\cos\dfrac{2\pi}{3} & 2\sin\dfrac{2\pi}{3} \end{bmatrix} \begin{bmatrix} J_a \\ J_b \end{bmatrix} = \sqrt{6}\boldsymbol{T}_{32} \begin{bmatrix} J_a \\ J_b \end{bmatrix}. \tag{10}$$

[2] Recall the Lorentz force equation $\mathbf{F} = \mathbf{J} \times \mathbf{B}$. Other terms in (6) and (7) are geometric constants.

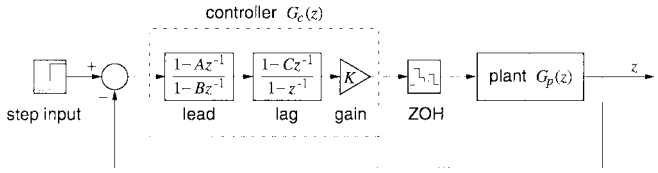

Fig. 5. Schematic diagram of the decoupled lead–lag controller.

The factor of $\sqrt{6}$ is introduced to match the definition of $[J_a \quad J_b]^T$. The transformation $\boldsymbol{T}_{32}$ is defined by

$$\boldsymbol{T}_{32} = \begin{bmatrix} \sqrt{\dfrac{2}{3}} & 0 \\ \dfrac{1}{\sqrt{6}} & \dfrac{1}{\sqrt{2}} \\ -\dfrac{1}{\sqrt{6}} & \dfrac{1}{\sqrt{2}} \end{bmatrix}. \tag{11}$$

The transformation matrix in the above has different elements from the usual inverse Blondel–Park transformation [14]. The difference arises from the phase current convention we are using, and the above representation is consistent with our previous work in [10].

Finally, the commutation law for the three-phase currents $[i_{kA} \quad i_{kB} \quad i_{kC}]^T$ and the desired forces $[f_{kz} \quad f_{k(x,\,y)}]^T$ becomes

$$\begin{bmatrix} i_{kA} \\ i_{kB} \\ i_{kC} \end{bmatrix} = \frac{2e^{\gamma_1 z_0}}{\mu_0 M_0 \eta_0 G N_m} \begin{bmatrix} 1 & 0 \\ 1/2 & \sqrt{3}/2 \\ -1/2 & \sqrt{3}/2 \end{bmatrix} e^{-\gamma_1 y_0 J} \cdot \begin{bmatrix} f_{kz} \\ f_{k(x,\,y)} \end{bmatrix}. \tag{12}$$

We now have a relationship between the desired forces and the phase currents.

IV. Linearized Equations of Motion

In this section, we derive linearized equations of motion for the vertical and lateral dynamics of the stage. They prove to be second-order dynamic equations with a mass and a (positive or negative) magnetic spring. To linearize these force equations, we set $z_0 = \overline{z}_0 + \tilde{z}_0$, $y_0 = \overline{y}_0 + \tilde{y}_0$, $i_d = \overline{i}_d + \tilde{i}_d$, and $i_q = \overline{i}_q + \tilde{i}_q$, where $\overline{z}_0$ is the nominal levitation height, which is 250 μm. From (8), the nominal direct current component $\overline{i}_d$ is calculated to be 500 mA, which generates 13.9 N per motor, about a quarter of the weight of the platen; four motors support the full platen weight of 54.7 N. The nominal quadrature current component $\overline{i}_q$ is zero, because the platen is in a dynamic equilibrium with $\overline{f}_{x,\,y} = 0$. The linearization in terms of the small-signal quantities with tilde is discussed later in this section.

A. Euler Angles

We need a transformation between the two coordinate systems—the body frame of the platen and the inertial frame of the stator. In other words, we describe the orientation of the body frame $x'y'z'$ with respect to the inertial frame xyz

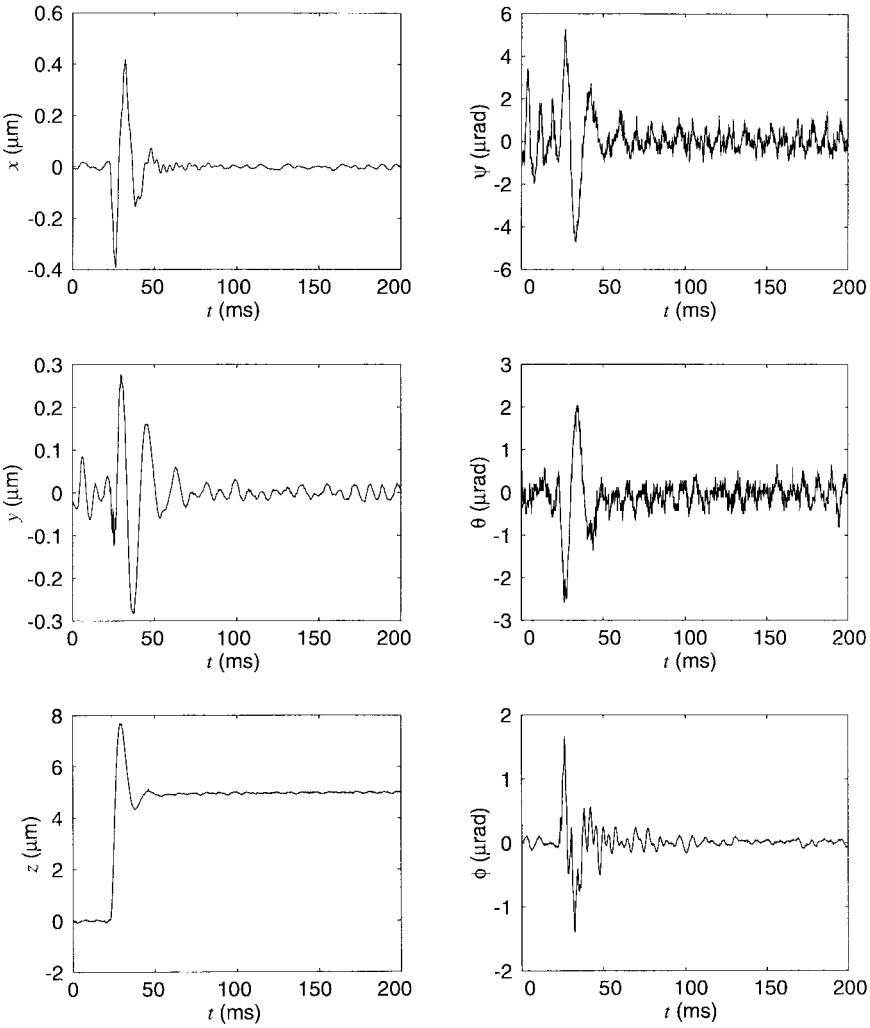

Fig. 6. 5-μm step response in z with perturbed motions in the other five axes.

defined in Fig. 2. We follow the xyz convention, which is commonly used in engineering applications, to define Euler angles [15]. Since the angular motions are small in our case, the Euler angles ψ, θ, and ϕ can be considered as rotations around the x, y, and z axes.

B. Equations of Motion

Retaining zeroth- and first-order terms, the equilibrium condition for the vertical direction becomes from (7)

$$f_z - Mg \cong 4 \cdot \tfrac{1}{2}\mu_0 M_0 \eta_0 N_m G \cdot (e^{-\gamma_1 \overline{z}_0}\overline{i}_d - \gamma_1 e^{-\gamma_1 \overline{z}_0}\overline{i}_d \tilde{z}_0 + e^{-\gamma_1 \overline{z}_0}\tilde{i}_d) \quad (13)$$

where f_z is the total vertical force, sum of f_{1z}, f_{2z}, f_{3z}, and f_{4z}. The factor of four in (13) results from assuming that the four linear motors are equally responsible for suspending the platen. When the platen is in dynamic equilibrium, the weight Mg of the platen should be matched by $4 \cdot (1/2)\mu_0 M_0 \eta_0 N_m G e^{-\gamma_1 \overline{z}_0}\overline{i}_d$. Now, the force equation becomes

$$f_z = 2\mu_0 M_0 \eta_0 N_m G e^{-\gamma_1 \overline{z}_0}\tilde{i}_d - 2\mu_0 M_0 \eta_0 N_m G \gamma_1 e^{-\gamma_1 \overline{z}_0}\overline{i}_d \tilde{z}_0. \quad (14)$$

So, the equation of incremental motion in the vertical direction is

$$M\frac{d^2\tilde{z}_0}{dt^2} + 2\mu_0 M_0 \eta_0 N_m G \gamma_1 e^{-\gamma_1 \overline{z}_0}\overline{i}_d \tilde{z}_0 = 2\mu_0 M_0 \eta_0 N_m G e^{-\gamma_1 \overline{z}_0}\tilde{i}_d. \quad (15)$$

When there is no control, $\tilde{i}_d = 0$, the vertical dynamics are marginally stable. The equation of incremental motion in the lateral direction is derived similarly [16], leading to

$$M\frac{d^2\tilde{y}_0}{dt^2} - \mu_0 M_0 \eta_0 N_m G e^{-\gamma_1 \overline{z}_0}\overline{i}_d \tilde{y}_0 = \mu_0 M_0 \eta_0 N_m G e^{-\gamma_1 \overline{z}_0}\tilde{i}_q. \quad (16)$$

When there is no control, $\tilde{i}_q = 0$, the lateral dynamics show its unstable nature.

With the levitator model in hand, we develop decoupled controllers in the next section.

V. Decoupled Vector Control

Classical decoupled lead–lag control is applied to stabilize the platen motion. We also provide test results on positioning noise and step responses in this section.

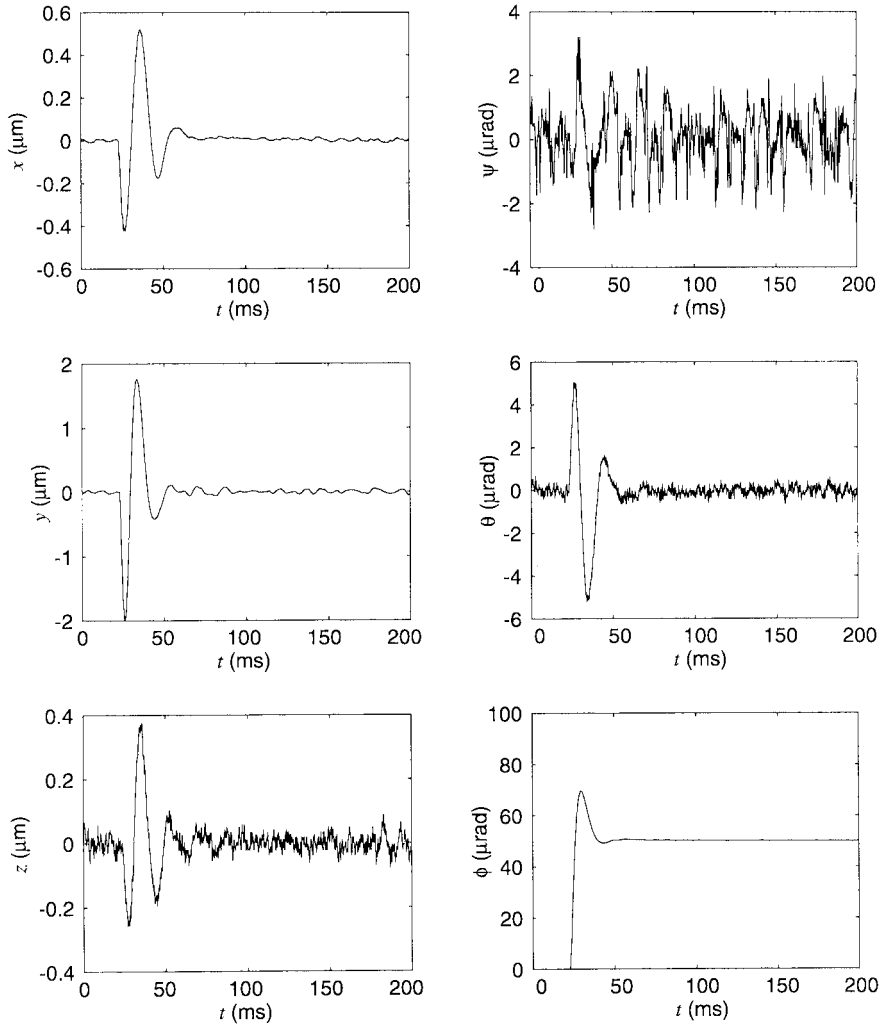

Fig. 7. 50-μrad step response in ϕ with perturbed motions in the other five axes.

A. Vertical Mode Control

By substituting nominal and geometric parameters given in Section III into (15), the decoupled vertical translational dynamics can be presented as

$$5.58\frac{d^2\tilde{z}}{dt^2} + 13\,600\tilde{z} = \tilde{f}_z. \tag{17}$$

The modal force $\tilde{f}_z$ is a sum of the decomposed vertical force components $\tilde{f}_{1z}$, $\tilde{f}_{2z}$, $\tilde{f}_{3z}$, and $\tilde{f}_{4z}$. The uncompensated resonant frequency of this platen mass-magnetic spring system is calculated as 7.85 Hz, which is very close to the measured natural frequency 8 Hz during testing.

To eliminate the steady-state error, the following lead–lag controller with a pole at the origin is implemented for z:

$$G_z(z) = 3.8006 \times 10^6 \frac{(1-0.96300z^{-1})(1-0.99624z^{-1})}{(1-0.68592z^{-1})(1-z^{-1})}. \tag{18}$$

The crossover frequency of this controller is 70 Hz. Fig. 5 is a block diagram of the closed-loop system with the controller. The phase margin of this controller is 51°, and it is fairly robust to force perturbations. Fig. 6 shows a 5-μm step response in z with this lead–lag controller.

Because of the geometrical symmetry in ψ and θ of the levitation system, they have identical controllers. These controllers are

$$G_{\psi,\theta}(z) = 3.6659 \times 10^4 \frac{(1-0.96300z^{-1})(1-0.99624z^{-1})}{(1-0.68592z^{-1})(1-z^{-1})}. \tag{19}$$

Their gains must be different from those in the $G_z(z)$, since the numerical values of the moments of inertia ($I_{xx} = I_{yy} = 0.0541$ kg-m^2) are different from those of the mass.

B. Lateral Mode Control

By substituting nominal and geometric parameters into (16), the decoupled lateral translational dynamics for the x direction

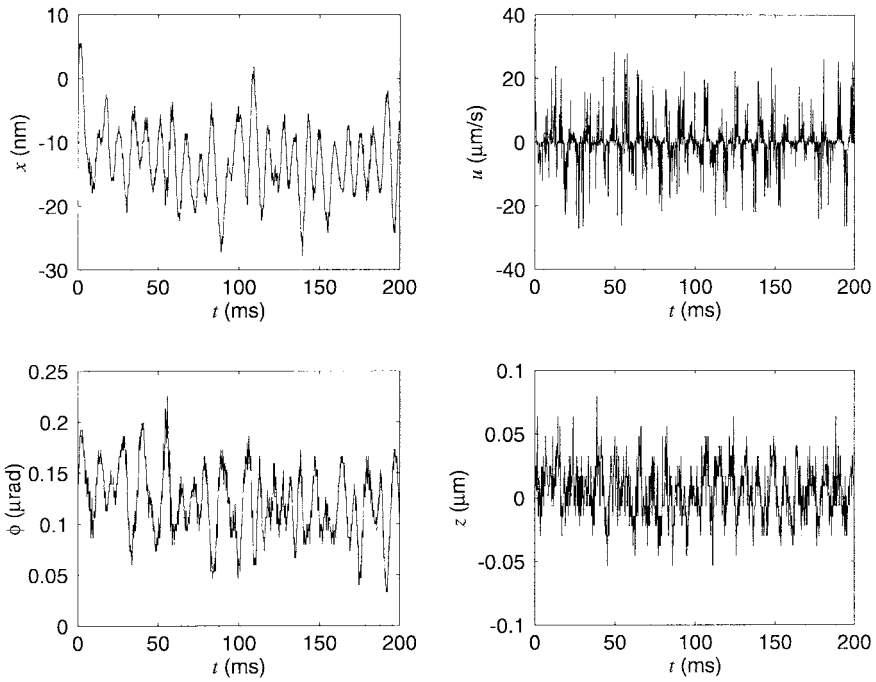

Fig. 8. Positioning noises in 6-DOF position regulation with the decoupled lead–lag controllers.

for motors I and III can be presented as[3]

$$5.58\frac{d^2\tilde{x}}{dt^2} - 27.71\tilde{x} = \tilde{f}_x. \tag{20}$$

The modal force $\tilde{f}_x$ is a sum of the decomposed lateral force components $\tilde{f}_{1x}$ and $\tilde{f}_{3x}$. Here, we again use the lead–lag controllers from (18) with a gain of 3.7047×10^6 N/m for x and y. Similarly, the controller for ϕ has the same pole–zero pattern as before with a gain of 6.4746×10^4 N/rad. Fig. 7 is a 50-μrad step response in ϕ. This completes the description of the decoupled control design for 6-DOF stabilization of the magnetic levitator.

C. Positioning Noise

Fig. 8 shows the position regulation under the decoupled lead–lag controllers designed above. The positioning noise[4] in x and y axes is on the order of 5 nm in the root-mean-square sense. The positioning noise in ϕ is 0.025 μrad rms. The test result in Fig. 8 contains a strong 120-Hz component. Laboratory floor vibration due to a large transformer in the laboratory, or heating, ventilation, and air-conditioning (HVAC) equipment located in the next room is believed to generate this noise. The figure also shows the vertical displacement z and the velocity u in the x direction. The vertical displacement shows a 15-nm-rms positioning noise in z. The noise of the A/D electronics used to sample the capacitance probe outputs is primarily responsible for the poorer positioning noise in z.

VI. Conclusions

In this paper, we have presented the modeling and vector control of our planar magnetic levitator. All the 6-DOF motions required for focusing and alignment in photolithography and large planar motions for positioning across the wafer surface can be generated by only one magnetically levitated moving part. Thus, the mechanical structure of the planar positioner is very simple. The actuators for the levitator are four surface-wound slotless permanent-magnet linear motors which exhibit no cogging force. The motors employ Halbach magnet arrays for power efficiency and low field distortion. Each of these actuators can generate vertical, as well as lateral, forces; it is a two-degree-of-freedom actuator.

We developed a dq theory for our two-degree-of-freedom actuator to decompose vertical and lateral force and current components. With this dq decomposition and transformations, we derived a commutation law to drive the four motors to stabilize and control the magnetically levitated platen. Linearized equations of motion were derived on the basis of the previous analysis [10]. A vector control was successfully realized for the planar magnetic levitator. We were able to stabilize the platen in 6-DOF, which confirmed the validity of our model and commutation law.

Decoupled real-time digital lead–lag controllers were designed and implemented with a digital signal processor. As test results, we presented step responses of the magnetically levitated stage. This levitator shows 5-nm-rms positioning noise and consumes only 5.4-W power per motor and is suitable

[3] We need to replace x with y for motors II and IV.

[4] We use the terminology *positioning noise* for uncertainty in position due to various disturbance and noise, such as electric noise in position sensors, A/D and D/A quantization, floor vibration, etc.

for the next-generation photolithography in semiconductor manufacturing.

APPENDIX
FORCE ALLOCATION

To implement decoupled digital controllers for 6-DOF stabilization of the platen, we derived force equations and decoupled the platen dynamics in Section IV. Since the current levitation stage is a redundant actuator system,[5] we need to allocate the modal forces and torques to the vertical and lateral decomposed forces.

A. Vertical Force Allocation

The force allocation can be derived with a free body diagram (Fig. 3) and dynamic equilibrium. The vertical force components should generate three-degree-of-freedom focusing and alignment motions, as well as support the mass of the platen (5.58 kg). So, the nominal vertical forces must satisfy

$$\overline{f}_{1z}+\overline{f}_{2z}+\overline{f}_{3z}+\overline{f}_{4z}=Mg=54.7\text{ N}. \tag{21}$$

By symmetry, the two large-signal vertical force components $\overline{f}_{1z}$ and $\overline{f}_{3z}$ are equal for the suspension purpose. It is arbitrarily chosen that together they carry half of the platen weight. So,

$$\overline{f}_{1z}=\overline{f}_{3z}=Mg/4. \tag{22}$$

Then, $\overline{f}_{2z}$ and $\overline{f}_{4z}$ support the remaining half of the platen weight according to

$$\overline{f}_{2z}+\overline{f}_{4z}=Mg/2. \tag{23}$$

Let us use another equilibrium condition for torques around the Y axis in Fig. 3. Since the moment arms of $\overline{f}_{1z}$, $\overline{f}_{2z}$, $\overline{f}_{3z}$, and $\overline{f}_{4z}$ are $\sqrt{2}(l_l-l_s)$, $\sqrt{2}l_s$, $\sqrt{2}(l_l-l_s)$, $\sqrt{2}l_l$, respectively,

$$(\overline{f}_{1z}+\overline{f}_{3z})(l_l-l_s)+\overline{f}_{4z}l_l=\overline{f}_{2z}l_s. \tag{24}$$

If we solve (21)–(24) for the force,

$$\begin{bmatrix}\overline{f}_{1z}\\ \overline{f}_{2z}\\ \overline{f}_{3z}\\ \overline{f}_{4z}\end{bmatrix}=\begin{bmatrix}1/4\\ \dfrac{2l_s-l_l}{2(l_s+l_l)}\\ 1/4\\ \dfrac{2l_l-l_s}{2(l_s+l_l)}\end{bmatrix}Mg=\begin{bmatrix}0.250\\ 0.333\\ 0.250\\ 0.167\end{bmatrix}Mg \tag{25}$$

where the platen center-of-mass offsets are $l_s=90.4$ mm, $l_l=113$ mm, and $l_s+l_l=203$ mm (8 in) is the distance between the centers of two adjacent magnet arrays. Thus, with the force–current relationship (8), the nominal direct components of the current are

$$\begin{bmatrix}\bar{i}_{1d}\\ \bar{i}_{2d}\\ \bar{i}_{3d}\\ \bar{i}_{4d}\end{bmatrix}=\begin{bmatrix}0.494\\ 0.658\\ 0.494\\ 0.331\end{bmatrix}\text{ A}. \tag{26}$$

[5]We have eight force components as in Fig. 2 in the current magnetic levitator. In fact, six independent force components are sufficient for 6-DOF motion control.

These equilibrium conditions are also valid for small-signal force components. Thus, we can use the same relations for the small-signal vertical force allocation.

$$\begin{bmatrix}\tilde{f}_{1z}\\ \tilde{f}_{2z}\\ \tilde{f}_{3z}\\ \tilde{f}_{4z}\end{bmatrix}=\begin{bmatrix}0.250\\ 0.333\\ 0.250\\ 0.167\end{bmatrix}\tilde{f}_z. \tag{27}$$

Since we do not want any net vertical force perturbation in equilibrium, therefore,

$$\tilde{f}_{1z}+\tilde{f}_{2z}+\tilde{f}_{3z}+\tilde{f}_{4z}=0. \tag{28}$$

Now consider the two other rotational degrees of freedom in the vertical dynamics. The modal torques have the following relationships with decomposed vertical force components:

$$\tilde{\tau}_x=(\tilde{f}_{1z}+\tilde{f}_{2z})l_s-(\tilde{f}_{3z}+\tilde{f}_{4z})l_l \tag{29}$$

$$\tilde{\tau}_y=(\tilde{f}_{4z}+\tilde{f}_{1z})l_l-(\tilde{f}_{2z}+\tilde{f}_{3z})l_s. \tag{30}$$

By the symmetry of the problem for the rotations around x and y axes,

$$\tilde{f}_{3z}=-\tilde{f}_{1z}. \tag{31}$$

Solving (28)–(31) for the force yields

$$\begin{aligned}\begin{bmatrix}\tilde{f}_{1z}\\ \tilde{f}_{2z}\\ \tilde{f}_{3z}\\ \tilde{f}_{4z}\end{bmatrix}&=\frac{1}{2(l_s+l_l)}\begin{bmatrix}\tilde{\tau}_x+\tilde{\tau}_y\\ \tilde{\tau}_x-\tilde{\tau}_y\\ -\tilde{\tau}_x-\tilde{\tau}_y\\ -\tilde{\tau}_x+\tilde{\tau}_y\end{bmatrix}\\ &=2.46\text{ m}^{-1}\begin{bmatrix}\tilde{\tau}_x+\tilde{\tau}_y\\ \tilde{\tau}_x-\tilde{\tau}_y\\ -\tilde{\tau}_x-\tilde{\tau}_y\\ -\tilde{\tau}_x+\tilde{\tau}_y\end{bmatrix}.\end{aligned} \tag{32}$$

Thus, the allocation of direct components of current is using (8)

$$\begin{bmatrix}\tilde{i}_{1d}\\ \tilde{i}_{2d}\\ \tilde{i}_{3d}\\ \tilde{i}_{4d}\end{bmatrix}=0.0889\text{ A/N-m}\begin{bmatrix}\tilde{\tau}_x+\tilde{\tau}_y\\ \tilde{\tau}_x-\tilde{\tau}_y\\ -\tilde{\tau}_x-\tilde{\tau}_y\\ -\tilde{\tau}_x+\tilde{\tau}_y\end{bmatrix}. \tag{33}$$

This completes the vertical force and current allocation with the modal vertical force and torques.

B. Lateral Force Allocation

The two relationships for the lateral force components are

$$\tilde{f}_x=\tilde{f}_{1x}+\tilde{f}_{3x} \tag{34}$$

$$\tilde{f}_y=\tilde{f}_{2y}+\tilde{f}_{4y}. \tag{35}$$

We need to generate the modal torque around the z axis with the four lateral force components. We have freedom to achieve this, and one choice is

$$\tilde{\tau}_z=\tilde{f}_{2y}l_s-\tilde{f}_{4y}l_l \tag{36}$$

$$0=\tilde{f}_{1x}l_s+\tilde{f}_{3x}l_l. \tag{37}$$

So, we generate $\tilde{\tau}_z$ with $\tilde{f}_{2y}$ and $\tilde{f}_{4y}$ only in the above force allocation. The force components, $\tilde{f}_{1x}$ and $\tilde{f}_{3x}$ do not

participate in the torque generation. Thus, the motors in the y direction will assume an additional task for small-angle adjustment around the z axis, which is also arbitrarily chosen.

Solving (34)–(37) for the force yields

$$\begin{bmatrix} \tilde{f}_{1x} \\ \tilde{f}_{2y} \\ \tilde{f}_{3x} \\ \tilde{f}_{4y} \end{bmatrix} = \frac{1}{l_s + l_l} \begin{bmatrix} \tilde{f}_x l_l \\ \tilde{f}_y l_l + \tilde{\tau}_z \\ \tilde{f}_x l_s \\ \tilde{f}_y l_s - \tilde{\tau}_z \end{bmatrix} = 4.93\ \mathrm{m}^{-1} \begin{bmatrix} 0.113\ \mathrm{m}\ \tilde{f}_x \\ 0.113\ \mathrm{m}\ \tilde{f}_y + \tilde{\tau}_z \\ 0.0904\ \mathrm{m}\ \tilde{f}_x \\ 0.0904\ \mathrm{m}\ \tilde{f}_y - \tilde{\tau}_z \end{bmatrix}. \quad (38)$$

Thus, the allocation of quadrature components of current is using (8)

$$\begin{bmatrix} \tilde{i}_{1q} \\ \tilde{i}_{2q} \\ \tilde{i}_{3q} \\ \tilde{i}_{4q} \end{bmatrix} = \begin{bmatrix} 0.0201\ \mathrm{A/N}\ \tilde{f}_x \\ 0.0201\ \mathrm{A/N}\ \tilde{f}_y + 0.178\ \mathrm{A/N\text{-}m}\ \tilde{\tau}_z \\ 0.0161\ \mathrm{A/N}\ \tilde{f}_x \\ 0.0161\ \mathrm{A/N}\ \tilde{f}_y - 0.178\ \mathrm{A/N\text{-}m}\ \tilde{\tau}_z \end{bmatrix}. \quad (39)$$

This completes the lateral force and current allocation with the modal lateral forces and torque.

REFERENCES

[1] G. Van Engelen and A. G. Bouwer, "Two-step positioning device using Lorentz forces and a static gas bearing," U.S. Patent 5 120 034, June 1992.

[2] S. Sakino, E. Osanai, M. Negishi, M. Horikoshi, M. Inoue, and K. Ono, "Movement guiding mechanism," U.S. Patent 5 040 431, Aug. 1991.

[3] S. Wittekoek and A. G. Bouwer, "Displacement device, particularly for the photolithographic treatment of a substrate," U.S. Patent 4 655 594, Apr. 1987.

[4] B. A. Sawyer, "Magnetic positioning device," U.S. Patent 3 376 578, Apr. 1968.

[5] W.-J. Kim and D. L. Trumper, "Force ripple in surface-wound permanent-magnet linear motors," in *Proc. IEEE Int. Magnetics Conf.*, Apr. 1996, p. FE-03.

[6] K. Halbach, "Design of permanent multipole magnets with oriented rare earth cobalt material," *Nucl. Instrum. Methods*, vol. 169, no. 1, pp. 1–10, 1980.

[7] D. L. Trumper, M. E. Williams, and T. H. Nguyen, "Magnet arrays for synchronous machines," in *Conf. Rec. IEEE-IAS Annu. Meeting*, Oct. 1993, pp. 216–223.

[8] K. Yoshida, J. Lee, and Y. J. Kim, "3-D FEM field analysis in controlled-PM LSM for maglev vehicle," *IEEE Trans. Magn.*, vol. 33, pp. 2207–2210, Mar. 1997.

[9] C. Barthod and G. Lemarquand, "Design of an actuator being both a permanent magnet synchronous motor and a magnetic suspension," in *Proc. IEEE Int. Magnetics Conf.*, Apr. 1997, p. BR–05.

[10] D. L. Trumper, W.-J. Kim, and M. E. Williams, "Design and analysis framework for linear permanent-magnet machines," *IEEE Trans. Ind. Applicat.*, vol. 32, pp. 371–379, Mar./Apr. 1996.

[11] W.-J. Kim, D. L. Trumper, and J. B. Bryan, "Linear-motor-levitated stage for photolithography," *Manuf. Technol.: Ann. CIRP*, vol. 46, no. 1, pp. 447–450, Oct. 1997.

[12] A. Blondel, *Synchronous Motors and Converters.* New York: McGraw-Hill, 1913, pt. III.

[13] R. H. Park, "Two-reaction theory of synchronous machines, generalized method of analysis—Part I," *Trans. AIEE*, vol. 48, no. 3, pp. 716–730, July 1929.

[14] A. E. Fitzgerald, C. Kingsley, Jr., and S. Umans, *Electric Machinery*, 5th ed. New York: McGraw-Hill, 1990, ch. 6.

[15] H. Goldstein, *Classical Mechanics.* Reading, MA: Addison-Wesley, 1980, ch. 4.

[16] W.-J. Kim, "High-precision planar magnetic levitation," Ph.D. dissertation, Dep. Elect. Eng. Comput. Sci., Massachusetts Inst. Technol., Cambridge, June 1997.

Won-jong Kim (S'89–M'97) was born in Seoul, Korea, in 1966. He received the B.S. (summa cum laude) and M.S. degrees in control and instrumentation engineering from Seoul National University, Seoul, Korea, in 1989 and 1991, respectively, and the Ph.D. degree in electrical engineering and computer science from Massachusetts Institute of Technology, Cambridge, in 1997.

In 1997, he joined SatCon Technology Corporation, Cambridge, MA, as a Member of the Technical Staff. His research interests are analysis, design, and control of electromechanical systems.

Dr. Kim received the Grand Prize in the Korean Institute of Electrical Engineers' Student Paper Contest in 1988 and the Gold Prize for his doctoral work from Samsung Electronics' Humantech Thesis Prize in 1997.

David L. Trumper (S'84–M'90) received the B.S., M.S., and Ph.D. degrees in electrical engineering and computer science from Massachusetts Institute of Technology, Cambridge, in 1980, 1984, and 1990, respectively.

In August 1993, he joined the Department of Mechanical Engineering, Massachusetts Institute of Technology, where he is currently the Rockwell International Career Development Associate Professor. Following receipt of the B.S. degree, he was with Hewlett-Packard Company for two years. Following receipt of the M.S. degree, he was with the Waters Chromatography Division, Millipore Corporation, for two years. Following receipt of the Ph.D. degree, he was an Assistant Professor in the Electrical Engineering Department, University of North Carolina, Charlotte, for three years, working in the Precision Engineering Group. His research interest is in the area of the control of electromechanical systems, with a specialization in magnetic suspensions and bearings. He serves on the Board of Directors of the American Society for Precision Engineering (ASPE).

Prof. Trumper is a member of the American Society of Mechanical Engineers, Society of Manufacturing Engineers, ASPE, and Japan Society for Precision Engineering and a corresponding member of the International Institution for Production Engineering Research.

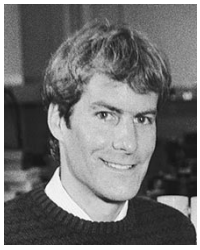

Jeffrey H. Lang (S'78–M'79–SM'95–F'98) received the B.S., M.S., and Ph.D. degrees in electrical engineering from Massachusetts Institute of Technology, Cambridge, in 1975, 1977, and 1980, respectively.

In 1980, he joined Massachusetts Institute of Technology, where he is currently a Professor of Electrical Engineering and Associate Director of the Laboratory for Electromagnetic and Electronic Systems. His research and teaching interests focus on the analysis, design, and control of electromechanical systems with an emphasis on rotating machinery, micro sensors and actuators, and flexible structures. He has authored more than 120 papers and is the holder of five U.S. patents in the areas of electromechanics, power electronics, and applied control. He is a former Hertz Foundation Fellow and a former Associate Editor of *Sensors and Actuators*.

Prof. Lang is the recipient of three IEEE Societies' Best Paper Prizes.